Experimental verification of the quasi-steady approximation for aerodynamic sound generation by pulsating jets in tubes

Zhaoyan Zhang, Luc Mongeau, and Steven H. Frankel
School of Mechanical Engineering, Purdue University, West Lafayette, Indiana 47907

(Received 17 October 2001; revised 28 May 2002; accepted 15 July 2002)

Voice production involves sound generation by a confined jet flow through an orifice (the glottis) with a time-varying area. Predictive models of speech production are usually based on the so-called quasi-steady approximation. The flow rate through the time-varying orifice is assumed to be the same as a sequence of steady flows through stationary orifices for wall geometries and flow boundary conditions that instantaneously match those of the dynamic, nonstationary problem. Either the flow rate or the pressure drop can then be used to calculate the radiated sound using conventional acoustic radiation models. The quasi-steady approximation allows complex unsteady flows to be modeled as steady flows, which is more cost effective. It has been verified for pulsating open jet flows. The quasi-steady approximation, however, has not yet been rigorously validated for the full range of flows encountered in voice production. To further investigate the range of validity of the quasi-steady approximation for voice production applications, a dynamic mechanical model of the larynx was designed and built. The model dimensions approximated those of human vocal folds. Airflow was supplied by a pressurized, quiet air storage facility and modulated by a driven rubber orifice. The acoustic pressure of waves radiated upstream and downstream of the orifice was measured, along with the orifice area and other time-averaged flow variables. Calculated and measured radiated acoustic pressures were compared. A good agreement was obtained over a range of operating frequencies, flow rates, and orifice shapes, confirming the validity of the quasi-steady approximation for a class of relevant pulsating jet flows.
[DOI: 10.1121/1.1506159]

PACS numbers: 43.70.Aj, 43.28.Ra [AL]

LIST OF SYMBOLS

A_g	glottal area (m^2)
A_t	tube cross-sectional area (m^2)
c	speed of sound (m/s)
C_d	dimensionless orifice discharge coefficient
d_t	tube inner diameter (m)
f	frequency (Hz)
G	Green's function
H	Heaviside function
k	wave number (m^{-1})
L	distance from the orifice (m)
P_{ij}	pressure stress tensor (Pa)
p	total pressure (Pa)
p'	unsteady pressure (Pa)
Q	instantaneous flow rate (m^3/s)
Q_0	mean flow rate (m^3/s)
R	reflection coefficient
Re	Reynolds number $Q_0 d_t / A_t \nu$
T_{ij}	Lighthill stress tensor
U	flow velocity (m/s)
U_c	centerline velocity (m/s)
u'	acoustic particle velocity (m/s)
v	orifice wall velocity (m/s)
Z_g	glottal impedance (Pa m^{-3}s)
Δp	instantaneous pressure drop across the orifice (Pa)
Δp_0	mean pressure drop across the orifice (Pa)
ρ_0	ambient density (kg/m^3)
ω	angular frequency (rad/s)
ν	kinematic viscosity (m/s^2)
σ_{ij}	viscous stress tensor

Subscripts

up	upstream
dn	downstream
0	time-averaged
c	centerline

I. INTRODUCTION

A good understanding of voice production is essential for many applications in speech sciences. For example, some physiological models for speech synthesis and recognition are based on articulatory parameters to model the speech production process (Gupta and Schroeter, 1993). Such physiological models of speech production may someday assist surgeons to predict the possible consequences of phonosurgery, or guide surgeons in the clinic. They may also allow more realistic speech synthesis and more effective speech recognition algorithms to be developed.

The basic mechanism of phonation is well understood, as described by Wegel (1930), Flanagan (1965), Titze (1973, 1974), and others. Airflow is expelled out from the lungs by contraction of the rib cage. Air flows through the bronchi, the trachea, and the vocal folds where it is modulated by the flow-induced vibrations of the vocal folds. A pulsating jet

flow is discharged into the supraglottal region, exciting acoustic waves within the vocal tract. The vibration of the glottis is driven by the periodic changes in the pressure gradient across the vocal folds. When the vocal folds are fully closed, the pressure on the upstream side is increased, and, after it reaches a threshold, forces the folds to open. As air flows out, the pressure gradient is decreased and the vocal folds are brought back together by the combination of a lower static pressure and elastic forces in the tissue. The cycle then repeats. The frequency of the vocal folds' oscillations determines the voice's pitch.

In the widely used source–filter model of speech production, the flow through the vocal folds is modeled as an ideal sound source, and the vocal tract acts as an acoustic filter (Flanagan, 1965). The source term is characterized by a nonlinear "glottal impedance," $Z_g(t)$, which is defined as the ratio of the transglottal pressure drop to the volume flow rate through the glottis. The characteristics of the acoustic filter depend on the instantaneous configuration of the vocal tract, such as the position of the tongue, teeth, lips, and velum. The glottal impedance is essential to the source–filter model. It is a time-varying quantity determined by many factors, including geometry, as well as inflow (subglottal) and outflow (supraglottal) boundary conditions. A detailed understanding of the flow field is required to calculate the glottal impedance from first principles.

The flows involved in the production of speech are essentially three-dimensional and turbulent (Alipour *et al.*, 1995). Three-dimensional simulations are needed to fully capture the detailed flow and acoustic fields. Recently, Zhao (2000) performed direct numerical simulations to investigate the sound production mechanisms in confined axisymmetric jet flows through modulated orifices. However, because the pulsating jet flows involve turbulence and flow separation and the glottal geometry is complex, it is prohibitively expensive to directly calculate the three-dimensional details of the flow and the acoustic fields simultaneously using computational methods.

The quasi-steady approximation is often made to simplify fluid flow analysis. It is assumed that the flow through a time-varying orifice can be simulated by a sequence of steady flows through orifices with the same geometry and boundary conditions as the time-varying orifice at specific time values. It is assumed that intrinsically unsteady effects related to flow acceleration or hysteresis can be neglected. The quasi-steady approximation allows the modeling of speech production as a sequence of steady flows, which are much easier to simulate than unsteady flows. The instantaneous glottal impedance can also be approximated by glottal impedances obtained directly from measurements using static physical models. The pressure–flow relationship in static physical models was studied first by Wegel (1930) and van den Berg *et al.* (1957), and empirical expressions were obtained for the glottal impedance. Many studies of static configurations, both experimental and computational, have since been reported (see, for example, Scherer *et al.*, 1983; Guo *et al.*, 1993).

Although it is widely used in speech-related applications, the quasi-steady approximation has not been thoroughly validated experimentally. The range of validity of the assumption is unknown for phonation (McGowan, 1993). Attempts have been made to investigate the flow field of confined jets flow through steady and pulsating orifices. Shadle *et al.* (1987) studied jet flow through a mechanically modulated orifice with a time-varying area. However, their studies were limited to flow visualization and static impedance measurements. So *et al.* (1987) investigated the near-field behavior of gas jets in a long tube. Iguchi *et al.* (1990) compared the properties of steady and pulsating confined jets through an orifice with constant area, and reported a difference in flow characteristics between acceleration phase and deceleration phase. Deviations from the quasi-steady approximation were observed also in the study of pulsating confined hydraulic jets by Diebold *et al.* (1990). Pelorson *et al.* (1994) and Pelorson (2001) have investigated flow separation phenomena and pressure–flow relationship for both steady and unsteady flows through constrictions in a duct. They showed that the pressure and flow velocity in unsteady flow predicted using the quasi-steady approximation was accurate, except for short instants prior to orifice closure and opening.

Mongeau *et al.* (1997) used a driven dynamic mechanical model in order to investigate the validity of the quasi-steady approximation for an open jet configuration. There was no tube downstream of the modulated rubber orifice. Furthermore, only one orifice shape, with convergent walls, was considered. The same question for confined pulsating jets, however, has not yet been addressed. In voicing, the geometry of the constriction between vocal folds varies during one cycle. The shape of the modulated orifice can be in turn divergent, straight, or convergent. This could induce significant changes in the flow dynamics, and may challenge the legitimacy of the quasi-steady approximation. The present study was aimed at extending the verification of the quasi-steady approximation for confined jet-flow configurations, and a few orifice geometries that are generically similar to the glottis during voicing.

II. THEORETICAL BACKGROUND

An idealization of the human larynx and the vocal tract as shown in Fig. 1(a). Air flows at low speed through an orifice in a rigid circular uniform tube.

A. Steady-state pressure–flow relationship

Consider first the case for which the orifice area does not change with time. For Reynolds numbers typical of phonation, the flow upstream and within the glottis is mostly laminar. Since the flow velocity is much smaller than the speed of sound, it is reasonable to assume an incompressible flow relation. Bernoulli's equation for a steady flow, along a streamline through the center of the orifice, yields

$$p_{\mathrm{up}} - p_{\mathrm{dn}} = \tfrac{1}{2}\rho_0 U_c^2, \tag{1}$$

where p_{up} and p_{dn} are the upstream and downstream pressure, respectively, ρ_0 is the ambient density, and U_c is the centerline flow velocity within the orifice. The volumetric flow rate could be obtained by integrating the axial velocity

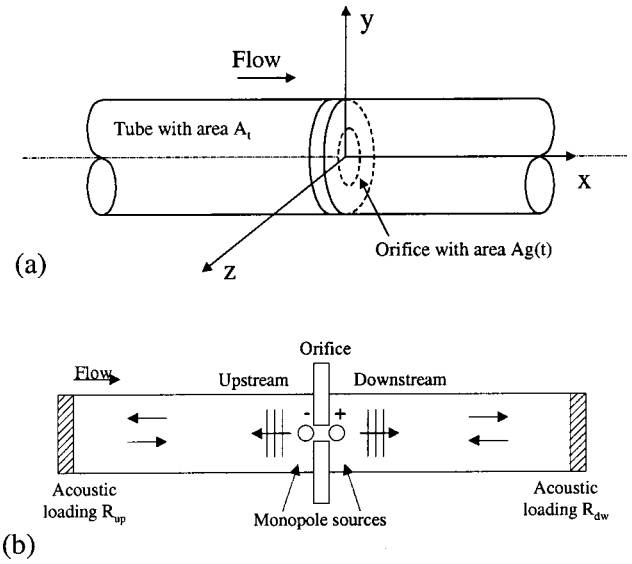

FIG. 1. (a) The coordinate system used in the model; (b) Acoustical representation of the physical model.

within the orifice over a plane normal to the tube axis (here the x axis)

$$Q=\int\int_{A_g} U(y,z)\cdot n_x dA_g, \tag{2}$$

where A_g is the orifice area. Due to the influence of viscosity near the walls, the flow velocity is not uniform over the cross section of the orifice. The orifice discharge coefficient is defined as

$$C_d=\frac{Q}{U_c A_g}. \tag{3}$$

Equation (2) can be rewritten in the following form, also known as Bernoulli's obstruction theory:

$$Q=C_d A_g U_c. \tag{4}$$

The orifice coefficient allows the effects of viscosity, of turbulence on the mean flow, of flow separation, and of orifice geometry to be accounted for. This parameter may be easily calculated from measured values of the pressure differential across the orifice, and the volumetric flow rate. Equations (1)–(4) provide the so-called steady pressure–flow relations which are the basis for quasi-steady models.

B. Quasi-steady approximation

If the quasi-steady approximation is valid, Eqs. (1) and (4) are then valid also for unsteady flow, with the variables in the equations representing the instantaneous values. For unsteady flow, the instantaneous pressure gradient across the orifice $\Delta p(t)$ can be decomposed into two components: a time-averaged pressure gradient Δp_0 and a time-varying component $(p'_{up}-p'_{dn})$. By substitution, Eq. (1) can be rewritten as

$$\Delta p(t)=\Delta p_0+p'_{up}(0^-,t)-p'_{dn}(0^+,t)=\tfrac{1}{2}\rho_0 U_c^2. \tag{5}$$

This formulation neglects intrinsically unsteady phenomena altogether. The unsteady form of Bernoulli's equation includes an additional flow acceleration term, i.e., the time derivative of the velocity potential. One might expect this term to contribute whenever large flow accelerations occur, such as when the glottis opens. Vortical structures shed by the orifice wall motion could persist over a significant period of time. They are convected at a rather low velocity (approximately one-half the centerline flow velocity), and thus they could alter the boundary condition downstream in the dynamic problem. The formation of a leading vortex (see, for example, Zhao *et al.*, 2000a) when the orifice impulsively transitions from a completely closed configuration (no flow through the orifice at all) to a fully developed jet is also an inherently unsteady phenomenon which would not appear in a steady flow. Whether or not these effects contribute significantly to sound radiation is the main question addressed in this study.

C. Acoustic source model

Strictly speaking, three major sound generation mechanisms contribute to the radiated sound, as explained in details by Zhao (2000) and Zhao *et al.* (2001b): (1) a quadrupole source related to kinetic energy fluctuations of the flow downstream of the orifice; (2) a monopole source due to the mass of the volume of air displaced by the motion of the orifice walls; and (3) a dipole source due to the unsteady axial forces exerted by the walls on the fluid. For conditions typical of human voice production, the dipole source is dominant among the three sound-generation mechanisms (more information about the formal acoustic analogy solution for this problem is provided in the Appendix). The dipole source radiates sound waves that are equal in magnitude and opposite in sign propagating upstream and downstream of the orifice.

Assuming low-frequency planar waves radiated in both directions from the orifice, one can always idealize the source region as a moving piston. Considering an observer located in the far field on either side of the piston, the piston can be modeled either as an equivalent monopole source or an equivalent dipole. The vocal-fold dimensions are small in comparison with the wavelengths of interest. The two segments of tissue are 1.0 to 1.5 cm in length for females, 1.8 to 2.2 cm for males, and 2 to 3 mm in thickness. For this study, the source region was idealized as two ideal, acoustically compact, one-dimensional equivalent monopoles. The pulsating flow radiates sound both downstream and upstream, with the corresponding monopole sources having equal strength and opposite (180°) phase [Fig. 1(b)]. Note again that these equivalent monopole sources are not the same as the classical ''displacement flow'' monopole according to Lighthill's acoustic analogy (an intrinsically nonstationary effect since its strength increases linearly with frequency). The equivalent monopole source strength includes all sound-generation mechanisms within the source region, believed to be dominantly dipole-like [see Eq. (A5)]. The reason for choosing a monopole rather than a dipole was to allow indirect verification of the quasi-steady assumption, as clarified in Sec. II E.

D. Sound wave reflections in tubes

Reflections occur as plane waves propagate through finite-length ducts. The influence of reflections can be modeled theoretically by adding image sources whose strength is determined from the acoustic loading at the end of each duct. The upstream and downstream sides of the orifice are considered separately, as illustrated in Fig. 1(b). Each system has its own monopole source located at the orifice. Each monopole source radiates into a rigid tube with a termination characterized by a reflection coefficient R. Plane-wave propagation is assumed considering the small tube diameter and the low fundamental frequency (below 200 Hz) of the orifice oscillations. The acoustic pressure p' both upstream and downstream can then be expressed as (Pierce, 1989)

$$p'(x,t) = \int B(x,\omega)\{e^{j(\omega t - k(L-x))} + R \cdot e^{j(\omega t + k(L-x))}\} d\omega, \tag{6}$$

where $B(x,\omega)$ is a function of position and frequency to be determined, x is the distance along the tube from the orifice, L is the tube length or the distance of the microphone from the source location, and ω and k are the angular frequency and wave number, respectively.

Using the one-dimensional equivalent monopole source model, the unsteady velocity at the source end is related to the unsteady flow rate through

$$u'_{\mathrm{up}}(0,t) = \int \frac{B_{\mathrm{up}}(0,\omega)}{\rho_0 c}\{e^{j(\omega t - kL)} - R \cdot e^{j(\omega t + kL)}\} d\omega = -\frac{1}{A_t}\{Q(t) - Q_0\}, \tag{7}$$

$$u'_{\mathrm{dn}}(0,t) = \int \frac{B_{\mathrm{dn}}(0,\omega)}{\rho_0 c}\{e^{j(\omega t - kL)} - R \cdot e^{j(\omega t + kL)}\} d\omega = \frac{1}{A_t}\{Q(t) - Q_0\}, \tag{8}$$

where u'_{up} and u'_{dn} are acoustic velocities in the upstream and downstream tubes, respectively, c is the speed of sound, A_t is the cross-section tube area, and Q_0 the time-averaged volumetric flow rate. The subtraction of Q_0 from the instantaneous flow rate inside the parenthesis is to remove the nonzero mean component of the particle velocities.

E. Verification procedure

The easiest way to verify predictions based on quasi-steady models would be to simultaneously measure transglottal pressure and flow rate for static and dynamic configurations. Unfortunately, the measurement of the instantaneous flow rate for the dynamic problem was not possible due to hardware limitations. An indirect method using radiated sound data and empirical static pressure–flow data was used instead. One advantage of this ''inverse filtering'' approach is that only the features of the flow that are responsible for sound radiation are accounted for. Any ''near-field'' effect (which would not contribute to speech production anyway) is automatically ignored. For this reason, it is advantageous to measure sound pressure away from the orifice. This, however, necessitates a deconvolution of the reflected waves and an iterative method of solution.

The procedure for the verification of the quasi-steady assumption is as follows. The upstream or downstream acoustic pressure was obtained by solving Eqs. (4), (5), (6), (7), and (8) simultaneously. First, initial values were selected for the upstream and downstream acoustic pressure, denoted by $p'^{1}_{\mathrm{up}}(0,t)$ and $p'^{1}_{\mathrm{dn}}(0,t)$, respectively. These were then substituted into Eq. (5) and U_c was obtained from the known (directly measured) Δp_0. The instantaneous flow rate, $Q(t)$, was then calculated from U_c and measured C_d and $A_g(t)$ values using Eq. (4). With $Q(t)$, $u'_{\mathrm{up}}(0,t)$, and $B_{\mathrm{up}}(0,\omega)$ calculated using Eq. (7), $p'^{i+1}_{\mathrm{up}}(0,t)$ was then determined using Eq. (6), where the superscript $i+1$ means the input for the $i+1$ iteration. The value of $p'^{i+1}_{\mathrm{dn}}(0,t)$ was determined in the same way using Eqs. (6) and (8). The quantity $p'^{i+1}_{\mathrm{up}}(0,t)$ was compared to its value at the previous iteration, $p'^{i}_{\mathrm{up}}(0,t)$. If the maximum difference was larger than a predetermined threshold value, i.e., $|\max[p'^{i+1}_{\mathrm{up}}(0,t) - p'^{i}_{\mathrm{up}}(0,t)]| > \varepsilon$, the iterations continued with $p'^{i+1}_{\mathrm{up}}(0,t)$ and $p'^{i+1}_{\mathrm{dn}}(0,t)$ as the input for the next iteration. Otherwise, the iterative process was stopped and $p'^{i+1}_{\mathrm{up}}(0,t)$ and $p'^{i+1}_{\mathrm{dn}}(0,t)$ yielded the final value for $p'_{\mathrm{up}}(0,t)$ and $p'^{i+1}_{\mathrm{dn}}(0,t)$, respectively.

To ensure numerical convergence, the acoustic pressure was filtered such that only the first few harmonic frequency components were retained. Frequency components above about 600 Hz were ignored. The filtering process was carried out in the frequency domain, every time Eq. (6), (7), or (8) was solved. Finally, $p'_{\mathrm{up}}(L,t)$ and $p'_{\mathrm{dn}}(L,t)$ were calculated using Eq. (6) for comparisons with experimental data.

This scheme relies on static pressure–flow relations in order to calculate the radiated sound pressure in the dynamic problem. Any shortcoming of the static relations would result in differences between the predicted and the directly measured radiated sound pressure, implying a failure of the quasi-steady approximation.

III. EXPERIMENTAL APPARATUS

A schematic of the experimental apparatus is shown in Fig. 2(a). A rubber orifice plate was built to simulate the human vocal-fold geometry, and acted as a constriction to the airflow. Three different orifice geometries (straight, convergent, and divergent) (Fig. 3) were used in the experiments. The orifice plates were molded using a liquid rubber with a room temperature vulcanized catalyst. During molding, two metallic driving rods were inserted within the rubber substrate such that they protruded from each side. These two rods were connected to an eccentric and a shaft entrained by an electric motor. Their movements were synchronized such that they moved in phase. The orifice was forced to open and close periodically at the desired frequency, adjusting the rotational frequency of the motor. Complete closure (with no leakage) was enforced over one portion of the cycle in all cases. The background mechanical noise generated by the motor and other moving parts was measured with the air supply turned off. This so-called ''background'' pressure signal actually included the displacement flow sound related to

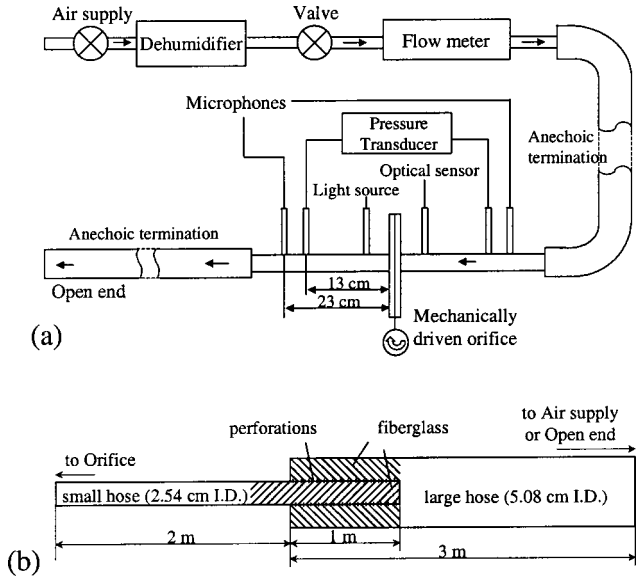

FIG. 2. Schematic of (a) experimental apparatus; (b) anechoic terminations.

the opening and closing of the orifice, which could not be distinguished from the mechanical noise. The amplitude of the background mechanical noise was found to be small compared with the sound generated by the pulsating flow inside the tube. The pressure signals associated with the measured background noise were nevertheless subtracted from measured sound pressures in the presence of airflow, with proper phase reference to the motion of the orifice. This procedure did not affect the signals significantly, as discussed later.

The orifice plate was inserted between two aluminum plates, which hosted the ends of the intake and discharge hoses. Two anechoic terminations were connected to the orifice plate on both sides to reduce possible reflections from either the air supply or the open end. Each anechoic termination was made of two overlapping sections of corrugated, rubber hoses with different inner diameters [Fig. 2(b)]. The smaller hose, having a 2.54-cm inner diameter, was connected directly to one aluminum plate at one end. Near the other end, the smaller hose was perforated and wrapped using fiberglass over a 1-m-long section. This end section was then inserted into a larger rubber hose with a 5.08-cm inner diameter. The junction was sealed to avoid any flow leakage.

The anechoic terminations were designed to minimize sound reflections from the upstream and downstream ends of the tubes. To evaluate their performance, the anechoic terminations (from the second microphone location) were treated as equivalent two-pole black box elements. The reflection factor was measured using the well-known two-microphone method (Seybert *et al.*, 1977). Microphones (B&K 4938), 6 mm in diameter, were mounted on each anechoic termination tube both upstream and downstream of the orifice, with one microphone mounted 13 cm from the orifice and another 23 cm from the orifice. The results are shown in Fig. 4. The measured reflection factor magnitudes of both upstream and downstream anechoic terminations vary between about 0.2 and 0.3 over most of the frequency range. The reflection factor is much larger at low frequency. Further reduction of the reflection factor at low frequency is very difficult with passive methods. The effects of reflection were suppressed using the convolution method discussed in Sec. II D.

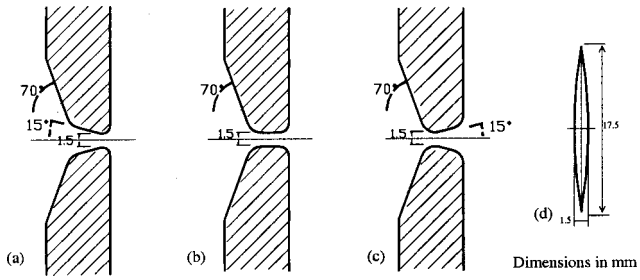

FIG. 3. Cross section of the three orifice passages: (a) convergent; (b) straight; and (c) divergent. The flow direction is from left to right. (d) elevation of the orifice showing the frontal opening area.

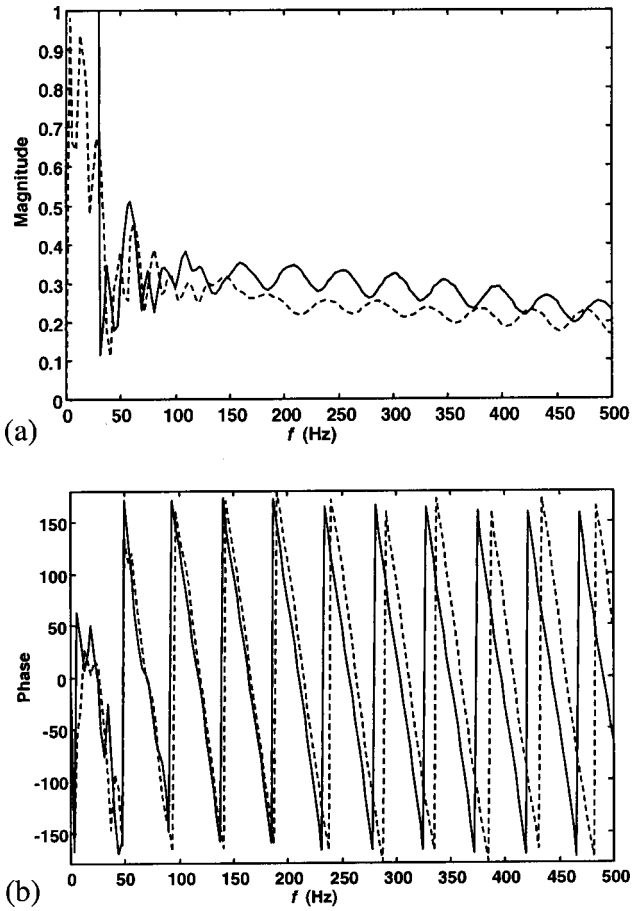

FIG. 4. Reflection factors of the upstream and downstream anechoic terminations. (a) magnitude; (b) phase. ———: upstream; – –: downstream.

To accurately measure the orifice area function, a photoelectric sensor and a light source were installed on opposite sides of the orifice, mounted on the tube walls. The photoelectric sensor signal was calibrated for different orifice openings, using the following approach. A picture of the orifice was made, with a scale placed close to the orifice opening. Numbers of pixels within the orifice opening and within the scale (the area of which was known *a priori*) were then counted using image-processing software. Their ratio is the ratio of the area of the orifice and that of the scale. The value of the orifice area was then calculated. The process was re-

peated nine times for nine different orifice openings. A linear relation between the output electric signal from the light sensor and the orifice area was found. A linear regression (with coefficient of determination $R^2=0.987$) between the light sensor output and the orifice area was obtained for subsequent data processing.

The volumetric flow rate was measured using a precision mass-flow meter (Baratron type 558A). The time-averaged pressure gradient across the orifice was measured using a pressure gauge (Baratron type 220C). The output signals from the microphones and the light sensor were acquired at a sampling rate of 16 384 Hz, using a HP356XA data acquisition system, and saved for subsequent analysis.

IV. RESULTS

The experiments were performed for three different orifice geometries, and mean pressure drops across the orifice of 6-, 9-, and 12-cm H_2O. The upstream and downstream acoustic pressures were recorded together with the mean flow rate through the orifice and the instantaneous orifice area. The experiments were performed at four different frequencies: 70, 80, 100, and 120 Hz. The experimental results for the convergent orifice geometry are discussed first.

A. Steady-state pressure–flow relationship

Steady pressure–flow relationships were obtained. The mean pressure drop across the orifice and the mean volume flow rate through the orifice were measured. The orifice discharge coefficients were then calculated from Eq. (3) and plotted against the Reynolds number, which is defined here based on the inner diameter of the smaller rubber hose d_t ($d_t=2.54$ cm)

$$\mathrm{Re}=\frac{Q_0 d_t}{A_t \nu}, \tag{9}$$

where ν is the kinematic viscosity. The results are shown in Fig. 5 for $\Delta p_0=12$ cm H_2O, and a convergent orifice geometry.

The orifice discharge coefficient increases with the Reynolds number for low Reynolds number flows. At higher Reynolds number, as the flow becomes more turbulent, the orifice discharge coefficient appears to asymptote to a value around 0.86. The pressure–flow relation was found to be repeatable. The effects of the orifice area A_g on the orifice discharge coefficient were found to be negligible (Mongeau *et al.*, 1997). A constant orifice discharge coefficient value of 0.86 was used in the predictions of the acoustic pressure for the convergent orifice (and a similar procedure was followed for the other shapes).

B. Orifice area

The orifice area during one cycle was measured using the photoelectric sensor. Figure 6 shows the orifice area at three different frequencies (80, 100, and 120 Hz), with $\Delta p_0=12$-cm H_2O and a convergent orifice geometry. The maximum orifice area function varied slightly for different frequencies. It generally increased over time during any test. This was most probably due to orifice deformation during the experiments. The duty cycle varied slightly with the orifice geometry. For the same geometry, the duty cycle remained nearly the same for different frequencies. The duty cycle was about 0.6 for the convergent orifice.

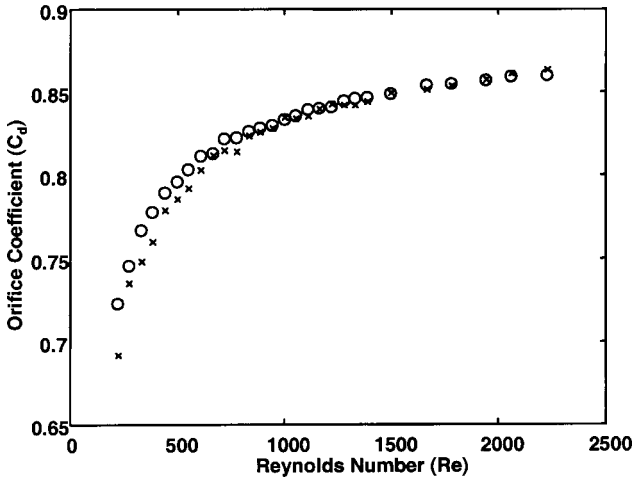

FIG. 5. Static pressure–flow relationship for the fully opened convergent orifice. The orifice discharge coefficient defined by Eq. (3) is plotted against the Reynolds number. Two sets of pressure-flow data were measured, before and after the experiments. xxx: before experiments; ooo: after experiments.

C. Unsteady flow measurements: Acoustic pressure and source volume velocity

Figure 7 shows the unsteady pressures measured upstream and downstream of the convergent orifice, with $f=80$ Hz, $\Delta p_0=12$-cm H_2O. The downstream unsteady pressure signal was multiplied by -1 to facilitate comparisons between upstream and downstream waveforms. Also shown in Fig. 7 are the upstream and downstream background noises measured in the absence of flow with the motor running at the same frequency. These are much smaller than the unsteady pressures with flow. This confirms that the displacement flow, which is included in the background noise, is negligible compared with the dipole contributions. The data were not corrected for the influence of reflections

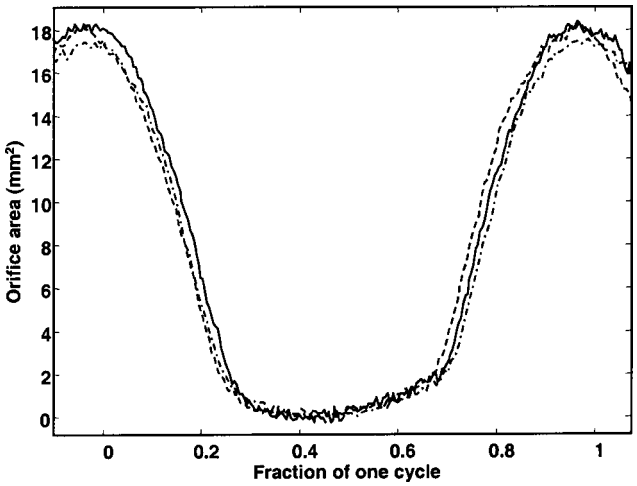

FIG. 6. Typical orifice area function during one cycle. $\Delta p_0=12$-cm H_2O, and convergent orifice geometry. ———: 80 Hz; – –: 100 Hz; — · — · —: 120 Hz.

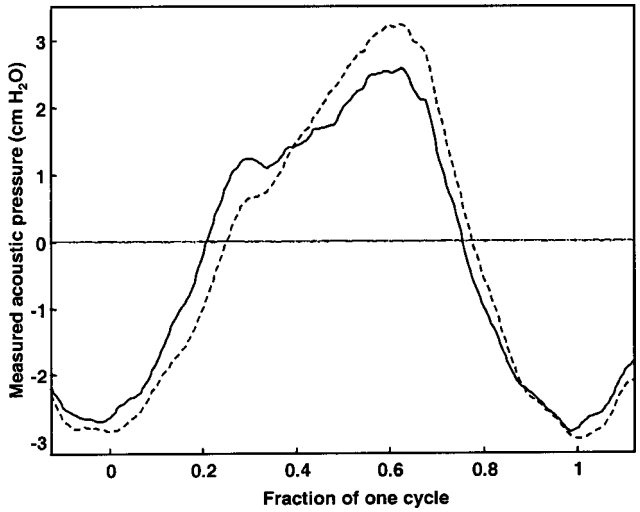

FIG. 7. The measured upstream and downstream unsteady pressure in the convergent orifice case. $f=80$ Hz, $\Delta p_0=12$-cm H_2O. ———: upstream; — —: downstream $\times(-1)$; – –: upstream background noise; --: downstream background noise.

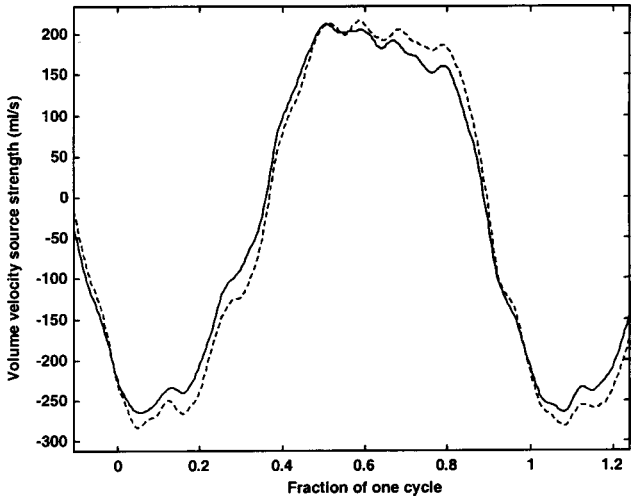

FIG. 8. Volume velocity source strength at the origin calculated based on the measured sound pressure and the reflection coefficient measured simultaneously at the same experiments. $f=80$ Hz, $\Delta p_0=12$-cm H_2O, and convergent orifice geometry. ——: upstream; – –: downstream $\times(-1)$.

off the tube ends in this case. Despite a slight phase difference, the upstream unsteady pressure is nearly perfectly 180° out of phase with the downstream unsteady pressure. The upstream unsteady pressure is generally out of phase with the orifice area (Fig. 6), while the downstream unsteady pressure is in phase with the orifice area, although both acoustic signatures have a slightly different shape from the orifice area function. This is consistent with the postulated dipole source model described in Sec. II.

The relative difference between the upstream and downstream measured sound pressure is quantified by a relative difference factor defined as

$$\Delta_p=\frac{\max(|(-p_{\mathrm{dn}})-p_{\mathrm{up}}|)}{\max(|p_{\mathrm{up}}|)}. \tag{10}$$

This error factor (11.95%) takes into account the possible differences in both the magnitude and the phase of the pressure signals.

The differences in the magnitude and phase between the upstream and downstream sound pressure here are primarily due to reflections from the tube ends at low frequency. As stated before, the upstream and downstream terminations can be modeled as two separate acoustic systems. These two acoustic systems should be excited by the same source strength amplitude according to the equivalent monopole source model. However, the reflection factors R vary with frequency and are different from each other (as shown in Fig. 4). Therefore, the unsteady pressures in these two acoustic systems, due to different standing wave patterns, are different.

Volume velocity sources originating at the orifice for the two acoustic systems should be more representative of source strength than the far-field pressure signals. The velocity source strength is defined as the acoustic volume flow rate at the location of the orifice. There are two volume velocity sources, one upstream and one downstream, each corresponding to one of the two acoustic systems. The source volume velocities can be calculated using Eq. (7) and Eq. (8), based on the measured sound pressure and the reflection coefficient of the corresponding anechoic termination. Figure 8 shows the comparison between the upstream and downstream source volume velocities obtained using the unsteady pressure data of Fig. 7. Again, the downstream velocity source was multiplied by -1 for comparison. The upstream velocity source has the same shape and magnitude as the downstream velocity source, 180° out of phase. Compared with unsteady pressure data, the source volume velocity waveform is more closely matched to the orifice area function. This high correlation confirms that the source of the measured unsteady pressure is mostly the dipole source due to pulsating airflow through the orifice rather than displacement flow due to orifice oscillations.

The relative difference between the upstream and downstream source volume velocities, evaluated as in Eq. (10), was 2.93% for this case. The upstream and downstream source volume velocities were in good agreement for all operating conditions. The relative difference for the volume velocity source strengths (2.93%) is smaller than that for the pressure (11.95%), which is expected as the effects of reflection were eliminated.

The same observations were made for other driving frequencies and mean pressure drops. The upstream and downstream source volume velocities were consistently found to be almost equal in strength and opposite in phase.

D. Quasi-steady model predictions

The upstream unsteady pressure was predicted following the method described in Sec. I E. The predicted upstream unsteady pressure is compared to the measured upstream unsteady pressure in Fig. 9. The frequency was 80 Hz, the mean pressure drop 12-cm H_2O, and the mean flow rate 221 ml/s. A constant convergent orifice discharge coefficient of 0.86 was used. The prediction, based on the quasi-steady approximation, agrees very well with the experimental data. The measured unsteady pressure waveform was successfully reconstructed from the orifice area function, including the

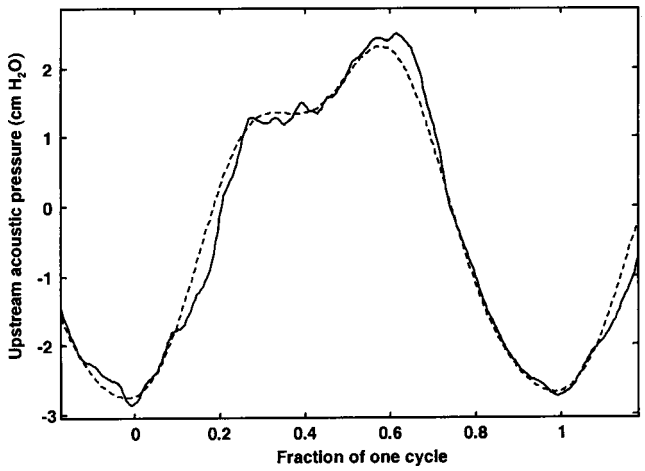

FIG. 9. Comparison between the measured upstream sound pressure and that predicted from the monopole source model and quasi-steady approximation. $f=80$ Hz, $\Delta p_0=12$-cm H_2O, and convergent orifice geometry. ———: measured; – –: predicted.

effects of reflections. The relative difference between the measured and predicted upstream sound pressure for different operating conditions, quantified by a relative error factor, was about 3.43%.

There are several possible causes for the discrepancies between the predictions and the measured data. In the predictions, the high-frequency components were discarded to ensure convergence of the iterative method. Evidently, high-frequency components are missing in the predictions. Second, as discussed before, the contributions of turbulence to both the dipole and quadrupole sources were neglected in this study. The model therefore could not capture their contributions, which are generally small and occur mostly at high frequency. The experimental determination of the reflection factors of the two anechoic terminations R is also a significant source of error. The reflection factors play an important role in the prediction procedure, and any error in this quantity is amplified by the iteration process.

The mean flow rate can be calculated from Eq. (4), with the centerline velocity U_c calculated from Eq. (5). The relative difference between the measured and predicted mean volumetric flows was about 2.58%, which was deemed acceptable.

A similar agreement was also obtained for the other operating conditions at different driving frequencies and mean pressure drops in the comparisons between the measured and predicted unsteady pressures and mean flow rates. At 100 Hz, the relative differences between the measured and predicted upstream acoustic pressure were less than 7.20%; the relative differences between the measured and predicted mean volumetric flow rates were less than 5.69%. At 120 Hz, the relative differences were less than 3.90% between the measured and predicted acoustic pressure, and less than 5.09% between the measured and predicted mean volumetric flow rates.

V. DISCUSSION

A. Influence of orifice geometry

The same measurements were repeated for straight and divergent orifice geometries at different operating conditions. The upstream and downstream unsteady pressures were measured, and the volume velocity of the source was deconvolved from the pressure data. The unsteady pressure was predicted based on the quasi-steady approximation and the equivalent monopole source model, and then compared to the experimental data. Typical results are shown in Fig. 10 and Fig. 11 for straight and divergent orifice geometries, respectively.

Good agreements between source volume velocities (within 3.5%), between measured and predicted pressures (within 7%), and between mean flow rate (within 8%) were obtained both for the straight and divergent orifice geometry cases. The effects of orifice geometry on the quasi-steady behavior were insignificant.

B. Influence of mean pressure drop

The influence of the mean pressure drop on sound production is governed by Bernoulli's equation. The amplitude of the generated sound should increase as the square root of the mean pressure drop [Eqs. (1), (4), and (8)]. Figure 12 shows the dimensionless volume velocity source strength for mean pressure drops of 6-, 9-, 12-cm H_2O. The data shown are for 120 Hz and the straight orifice geometry. The source volume velocity was nondimensionlized using the square root of the mean pressure drop across the orifice. The good collapse of the data also justifies the application of Bernoulli's obstruction theory for steady flow, on which the quasi-steady approximation lies. The slight discrepancy is believed to be due to experimental errors.

C. Influence of frequency

According to the quasi-steady approximation, frequency should have no effect on the sound pressure if the effects of acoustic loading are neglected. The presence of reflections, however, causes a frequency dependent acoustic loading. This colors the acoustic signatures, both upstream and downstream, as shown in Fig. 13(a). In contrast, the source volume velocity should be less dependent, if not independent, of frequency. Figure 13(b) shows the velocity sources at different frequencies, with the mean pressure drop across the orifice kept at 12-cm H_2O (for the straight orifice geometry). The figure shows a reduced dependence of the velocity source strength on the frequency, as expected. The discrepancies are believed to be due mostly, to errors in the reflected wave deconvolution process.

D. Unsteady effects and acoustical resonance

The quasi-steady approximation neglects the effects of flow acceleration and deceleration. These effects might be important at the short instants prior to orifice abrupt closure and opening, at which the derivative of the flow velocity is very large. Bernoulli's equation may not be valid for these

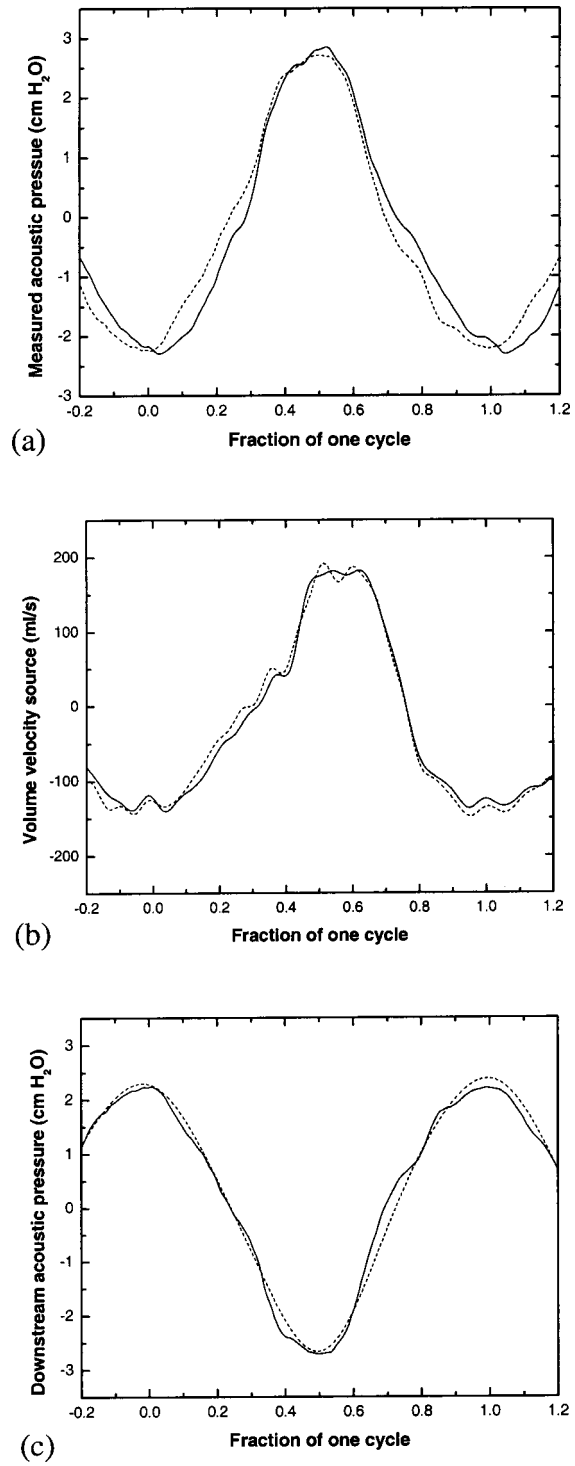

FIG. 10. Experimental results and analysis for straight orifice geometry. $f=120$ Hz, $\Delta p_0=12$-cm H_2O. (a) measured unsteady pressure upstream and downstream of the orifice, with the downstream unsteady pressure multiplied by minus 1 for convenient comparison. ——: upstream; — —: downstream $\times(-1)$. (b) calculated volume velocity source strength, both upstream and downstream. The downstream is again multiplied by minus 1. ——: upstream; — —: downstream $\times(-1)$. (c) comparison between the measured and predicted downstream acoustic pressure. ——: measured; — —: predicted.

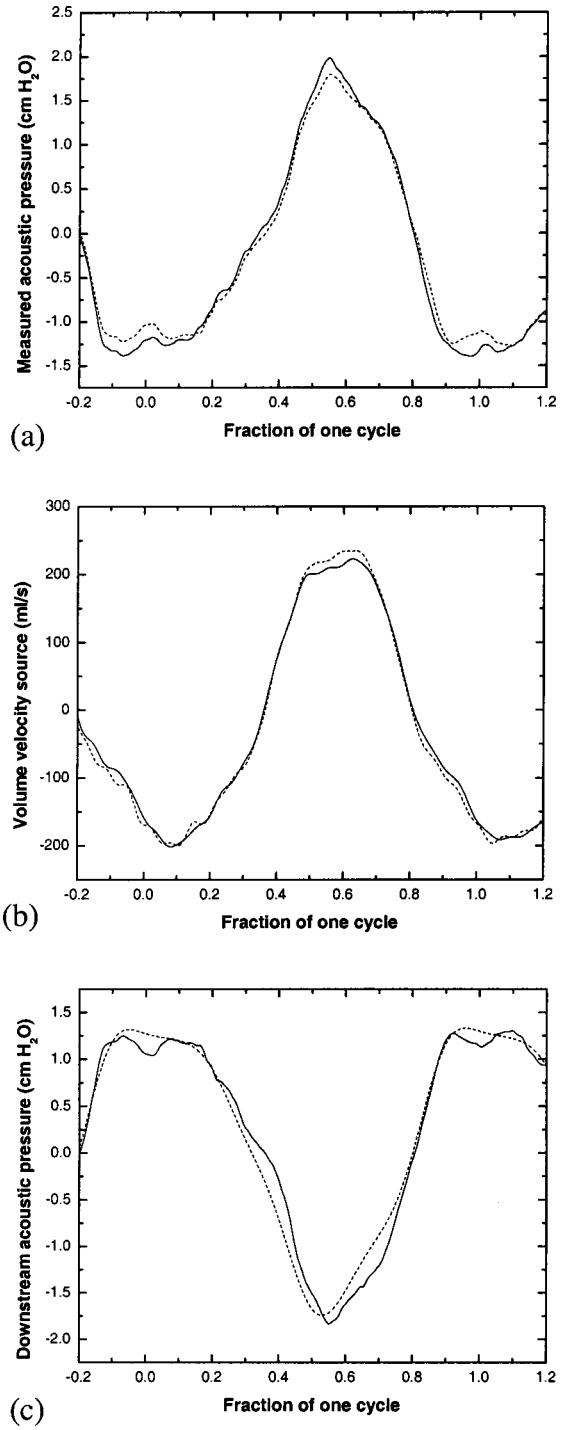

FIG. 11. Experimental results and analysis for divergent orifice geometry. $f=100$ Hz, $\Delta p_0=12$-cm H_2O. (a) measured unsteady pressure upstream and downstream of the orifice, with the downstream unsteady pressure multiplied by minus 1. ——: upstream; — —: downstream $\times(-1)$. (b) volume velocity source strength, both upstream and downstream, with the downstream curve again multiplied by minus 1. ——: upstream; — —: downstream $\times(-1)$. (c) comparison between the measured and predicted downstream unsteady pressure. ——: measured; — —: predicted.

short instants, and viscous effects and acoustic near field must be accounted for to accurately model the flow and sound radiation (Mongeau *et al.*, 1997).

Another situation at which deviations from the quasi-steady behavior may be significant is when the orifice is driven at the formant frequency. Although acoustic effects and source behavior are generally considered to be independent, they are in many ways coupled by a nonlinear relationship between instantaneous transglottal pressure and flow rate. It is anticipated that for frequencies corresponding to

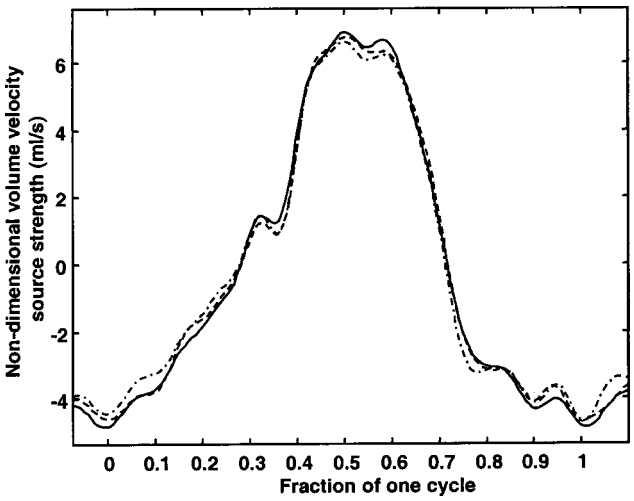

FIG. 12. Volume velocity source strengths at 120 Hz for three different mean pressure drops (6-, 9-, 12-cm H_2O), and straight orifice geometry. The volume velocity source strength is scaled by the square root of the mean pressure drop. ——: 12-cm H_2O; — —: 9-cm H_2O; ---: 6-cm H_2O.

the resonance frequencies of the subglottal tube, there will be a pressure node at the location of the glottis. The transglottal pressure therefore should vanish, or even become negative. It is possible that at resonance some reverse flow might then occur during parts of one glottal cycle, severely distorting the pulsating jet flow behavior. The comparative magnitude of the dipole and monopole contributions may therefore be different. This will be the object of future work.

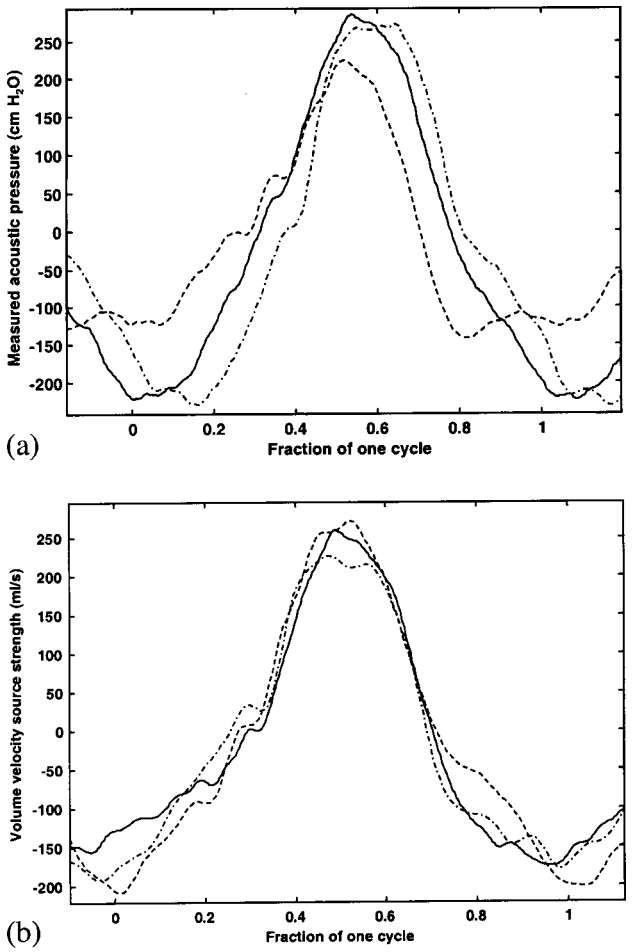

FIG. 13. Volume velocity source strengths for different frequencies. Δp_0 = 12-cm H_2O, convergent orifice geometry. (a) measured sound-pressure data. (b) corresponding volume velocity source strength. ——: 70 Hz; — —: 100 Hz; ---: 120 Hz.

VI. CONCLUSION

The quasi-steady approximation was validated for the tonal component of sound generated by pulsating confined jets. Experiments were performed over the fundamental frequency range extending from 70 to 120 Hz. The radiated unsteady pressure predicted using the quasi-steady approximation and a one-dimensional sound radiation model was found to be in good agreement with experimental data. This implies that monopole and quadrupole components are negligible compared with dipole source mechanisms in pulsating flows (as in voiced sound production), at least at frequencies below a few kilohertz. The orifice oscillation frequency was found to have little effect on dipole sound source strength. Different orifice geometries (straight, convergent, and divergent orifices) simulating the glottis at three different stages during phonation were investigated. The effects of orifice geometry on the quasi-steady behavior of dipole sound generation in unsteady flow were insignificant.

ACKNOWLEDGMENTS

This study was supported by Research Grant No. 5 RO1 DC03577-04 from the National Institute of Deafness and Other Communication Disorders, National Institutes of Health.

APPENDIX: SOUND SOURCES IN SPEECH PRODUCTION

The sound generation mechanisms in confined flows through oscillating orifices may be described theoretically using the Ffowcs Williams–Hawkings (FWH) equation (Ffowcs Williams and Hawkings, 1969). To define the different domains of interest, a detailed view of the presumed source region (around the orifice) is shown in Fig. 14. The fixed cylindrical control volume V' consists of the orifice section, together with the upstream and downstream tubes, including the deformable part of the orifice walls. The source region V includes only the gas within the orifice, and it has a moving boundary. Ideal planar acoustic waves are assumed upstream and downstream of the source region. An observer, or ''virtual microphone,'' is placed in the acoustic far field inside the control volume V', but outside the source region V. The observer can be on either side of the orifice. The

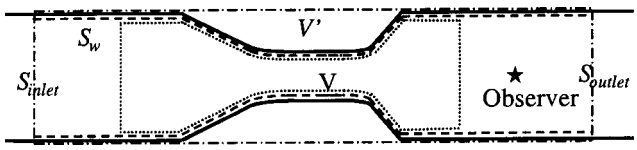

FIG. 14. Integral domains and surfaces for the application of the Ffowcs Williams–Hawkings equation.

surface delimiting the position of the walls is denoted by S_w, with the normal unit vector pointing into the fluid. The FWH equation is

$$\left\{\frac{\partial^2}{\partial\tau^2}-c_0^2\nabla^2\right\}[H(S)\rho'] = \frac{\partial^2}{\partial y_i\partial y_j}[T_{ij}H(S)]-\frac{\partial}{\partial y_i}[F_i\delta(S)]+\frac{\partial}{\partial\tau}[Q\delta(S)], \tag{A1}$$

where $H(S)$ is the Heaviside function, $\delta(S)$ is the Dirac function, and $S(y,\tau)$ is a function describing the geometry of the wall boundary. It is assumed that $S>0$ in the flow region, $S<0$ outside the flow region, and $S=0$ on the boundary. The quantities on the right-hand side of the equation are given by

$$T_{ij}=\rho u_i u_j+\delta_{ij}(p_0+p'-c_0^2\rho')-\sigma_{ij}, \tag{A2}$$

$$F_i[p\,\delta_{ij}-\sigma_{ij}+\rho u_i(u_j-v_j)]\frac{\partial S}{\partial y_j}, \tag{A3}$$

$$Q=[\rho_0 v_i+\rho(u_i-v_i)]\frac{\partial S}{\partial y_i}, \tag{A4}$$

where v_j is the wall velocity, σ_{ij} is the viscous stress tensor, and $\rho'=\rho-\rho_0$ is the fluctuating density.

Assuming a no-slip condition on the wall boundary, and adiabatic compression and rarefaction, the solution to the FWH equation for one-dimensional plane wave propagation in a duct may be written as

$$\begin{aligned} p'(x,t)=&\frac{1}{2A_0c_0}\frac{\partial}{\partial t}\int_V[\rho u_1^2-\sigma_{11}]_{t*}dV && \text{(I)}\\ &-\frac{1}{2A_0}\int_{S_w}[p'\delta_{1j}-\sigma_{1j}]_{t*}n_j \\ &\times\text{sign}(x_1-y_1)dS && \text{(II)}\\ &-\frac{1}{2A_0}\int_{S_w}[\rho_0c_0v_j]_{t*}n_j\,dS && \text{(III)}\\ &+\frac{1}{2A_0}\int_{S_{\text{inlet}}}[c_0^2\rho'+\rho c_0u_1]_{t*}dS && \text{(IV)}\\ &+\frac{1}{2A_0}\int_{S_{\text{outlet}}}[c_0^2\rho'-\rho c_0u_1]_{t*}dS, && \text{(V)} \end{aligned} \tag{A5}$$

where n_j is a unit normal vector directed outwards the flow region, **x** and **y** are the observer and source positions, respectively, $t^*=t-|x_1-y_1|/c_0$ is the retarded time, and V is the source region.

Contributions from four types of sources may be identified. Term I is a quadrupole source related to the turbulent flow and viscous stress inside the tube, specifically the kinetic energy of the fluctuating flow motion along the direction of wave propagation. Term I may be comparatively large when the flow is turbulent. Term II is a dipole source due to the unsteady forces exerted by the walls onto the fluids. The viscous stress components in both terms I and II may be ignored (Zhao, 2001b). Term III is a monopole source due to the motion of the orifice walls. It is sometimes referred to as a "displacement flow." Terms IV and V are monopole sources enforced at the inlet and outlet boundaries. Since the inlet and outlet boundaries are located in the acoustic region, these two monopole sources are image sound sources arising from the interactions between radiated sound waves with the outer boundaries of the domain V'. If the tubes were perfectly anechoically terminated, there would be no reflection from both the inlet and outlet, and terms IV and V would vanish. In the case of imperfect anechoic termination they can be accounted for using a convolution method, as discussed in Sec. II D.

Turbulence may contribute to sound generation, specifically through terms I and II. Term I is the Reynolds stress in the direction of wave propagation. The fluctuating pressure due to turbulence contributes to term II as well. The turbulence-generated sound is mostly of high frequency, and is important to speech quality. However, its magnitude is much smaller than the sound generated by tonal source components. It may therefore be neglected as a first approximation. The contribution of turbulence was the object of a separate study (Zhang *et al.*, 2002).

Based on the above assumptions, Eq. (A5) shows that unsteady flow and orifice wall motion give rise to two types of sound-generation mechanisms. The monopole source, term III, is induced entirely by the oscillation of the orifice wall. Its magnitude increases with orifice velocity, and therefore increases with oscillation frequency. The dipole contribution, term II, is due to the net unsteady force exerted by the walls onto the fluid in the direction of sound wave propagation. It is governed by the pressure drop (or Bernoulli head loss) across the orifice induced largely by the unsteady flow through the orifice, with a very small contribution from the acceleration of the walls. Recent numerical studies of comparable flows (Zhao, 2000; Zhao *et al.*, 2000a, 2000b, 2001a, 2001b) showed that when there is no externally imposed unsteady flow, both the quadrupole term and the dipole term are negligible compared with term III, the monopole source. When an externally imposed unsteady flow is present, however, the dipole source becomes significantly large, as the fluctuating pressure on the walls increases. The monopole source strength was found to increase with the orifice oscillation frequency, while the dipole source contribution remained nearly unchanged as the frequency was varied (Zhang *et al.*, 2001). Therefore, at low frequencies and for an externally imposed unsteady flow, the dipole source dominates, and most of the energy of the radiated sound comes from the unsteady flow contribution in the dipole term. The effects of wall motion are significant only at high frequencies.

In human speech, where unsteady airflow is present, the typical value of fluctuating velocity in glottis is of the order of 40 m/s, and the associated pressure drops are of the order $\frac{1}{2}\rho_0U_c^2\sim 1$ kPa. This value is much larger than the velocity of the vocal-fold walls, which is of the order of 0.1 m/s (for a pitch frequency about 100 Hz and a 2-mm vocal-fold displacement). For planar waves, $p'=\rho_0c_0u'$ and the monopole source pressures ($\sim$45 Pa) are negligible in this case. Therefore, the dipole source is dominant, at least at low frequencies.

Alipour, F., and Scherer, R. C. (**1995**). ''Pulsatile airflow during phonation: An excised larynx model,'' J. Acoust. Soc. Am. **97**, 1241–1248.
Diebold, B., Delouche, A., Dumee, PH., Guglielmi, J.-P., Delouche, P., and Peronneau, P. (**1990**). ''*In vitro* analysis of a model of intracardiac jet: Analysis of the central core of axisymmetric jets,'' J. Biomech. **23**, No. 1, 35–44.
Ffowcs Williams, J. E., and Hawkings, D. L. (**1969**). ''Sound generation by turbulence and surfaces in arbitrary motion,'' Philos. Trans. R. Soc. London, Ser. A **264**, 321–342.
Flanagan, J. L. (**1965**). *Speech Analysis, Synthesis, and Perception* (Springer, Berlin).
Guo, C. G., and Scherer, R. C. (**1993**). ''Finite element simulation of glottal flow and pressure,'' J. Acoust. Soc. Am. **94**, 688–700.
Gupta, S. K., and Schroeter, J. (**1993**). ''Pitch-synchronous frame-by-frame and segment-based articulatory analysis by synthesis,'' J. Acoust. Soc. Am. **94**, 2517–2530.
Iguchi, M., Yamazaki, H., Yamada, E., and Morita, Z. (**1990**). ''Velocity and turbulence intensity in a pulsating jet through a sudden expansion,'' Trans. Jpn. Soc. Mech. Eng. **56**, 1659–1664.
McGowan, R. S. (**1993**). ''The quasisteady approximation in speech production,'' J. Acoust. Soc. Am. **94**, 3011–3013.
Mongeau, L., Franchek, N., Coker, C. H., and Kubli, R. A. (**1997**). ''Characteristics of a pulsating jet through a small modulated orifice, with application to voice production,'' J. Acoust. Soc. Am. **102**, 1121–1133.
Pelorson, X. (**2001**). ''On the meaning and accuracy of the pressure-flow technique to determine constrictions within the vocal tract,'' Speech Commun. **35**, 179–190.
Pelorson, X., Hirschberg, A., van Hassel, R. R., Wijnands, A. P. J., and Auregan, Y. (**1994**). ''Theoretical and experimental study of quasi-steady flow separation within the glottis during phonation. Application to a modified two-mass model,'' J. Acoust. Soc. Am. **96**, 3416–3431.
Pierce, A. D. (**1989**). *Acoustics: An Introduction to its Physical Principles and Applications* (American Institute of Physics, New York).
Scherer, R. C., Titze, I. R., and Curtis, J. F. (**1983**). ''Pressure-flow relationships in two models of the larynx having rectangular glottal shapes,'' J. Acoust. Soc. Am. **73**, 668–676.
Seybert, A. F., and Ross, D. F. (**1977**). ''Experimental determination of acoustic properties using a two-microphone random-excitation technique,'' J. Acoust. Soc. Am. **61**, 1362–1370.
Shadle, C. H., Elliott, S. J., and Nelson, P. A. (**1987**). ''Visualization of the air flowing through a dynamic model of the vocal folds,'' ISVR Technical Report 154.
So, R. M. C., Ahmed, S. A., and Yu, M. H. (**1987**). ''The near-field behavior of turbulent gas jets in a long confinement,'' Exp. Fluids **5**, 2–10.
Titze, I. R. (**1973**). ''The human vocal cords: A mathematical model. I,'' Phonetica **28**, 128–170.
Titze, I. R. (**1974**). ''The human vocal cords: A mathematical model. II,'' Phonetica **29**, 1–21.
van den Berg, J. W., Zantema, J. T., and Doomenbal, P. (**1957**). ''On the air resistance and the Bernoulli effect of the human larynx,'' J. Acoust. Soc. Am. **29**, 626–631.
Wegel, R. L. (**1930**). ''Theory of vibration of the larynx,'' Bell Syst. Tech. J. **9**, 207–227.
Zhang, C., Zhao, W., Frankel, S. H., and Mongeau, L. (**2001**). ''Computational aeroacoustics of phonation: Effect of subglottal pressure, glottal oscillation frequency, and ventricular folds,'' J. Acoust. Soc. Am. **109**, 2412.
Zhang, Z., Mongeau, L., and Frankel, S. H. (**2002**). ''Broadband sound generation by confined turbulent jets,'' J. Acoust. Soc. Am. **112**, 677–689.
Zhao, W. (**2000**). ''A numerical investigation of sound radiated from subsonic jets with application to human phonation,'' Ph.D. thesis, Purdue University, West Lafayette, Indiana.
Zhao, W., Frankel, S. H., and Mongeau, L. (**2000a**). ''Effects of trailing jet instability on vortex ring formation,'' Phys. Fluids **12**, No. 3, 589–596.
Zhao, W., Frankel, S. H., and Mongeau, L. (**2000b**). ''Effects of spatial filtering on sound radiation from a subsonic axisymmetric jet,'' AIAA J. **38**, No. 11, 2032–2039.
Zhao, W., Frankel, S. H., and Mongeau, L. (**2001a**). ''Large eddy simulation of sound radiation from subsonic turbulent Jets,'' AIAA J. **39**, No. 8, 1469–1477.
Zhao, W., Frankel, S. H., and Mongeau, L. (**2001b**). ''Numerical simulations of sound from confined pulsating axisymmetric jets,'' AIAA J. **39**, No. 10, 1868–1874.